Research Article

Ryoji Katsube* and Yoshitaro Nose

Synthesis of alkaline-earth Zintl phosphides MZn_2P_2 (M = Ca, Sr, Ba) from Sn solutions

https://doi.org/10.1515/htmp-2022-0019
received September 29, 2021; accepted January 04, 2022

Abstract: Exploration of suitable partner materials (so-called buffer layer or n-type emitter) for each light-absorbing material is essential to practicalize various emerging photovoltaic devices. Motivated by our recent discovery of a partner material, $Mg(Mg_xZn_{1-x})_2P_2$, in Mg/Zn_3P_2 solar cells, the related series of materials MZn_2P_2 (M = Ca, Sr, Ba) is of interest to the application in pnictide-based solar cells. In this study, we synthesize these materials to evaluate the optoelectronic properties concerning photovoltaic applications. To deal with the difficulties of the high vapor pressure and reactivity of the constituent elements, we utilized Sn as a solvent to reduce their activities during heat treatments. Powders that are mainly composed of MZn_2P_2 were obtained by crushing the samples after solution growth, although single-phase crystals of MZn_2P_2 could not be obtained in this study. The optical bandgap and the ionization potential of each MZn_2P_2 were evaluated through the diffuse reflectance and the photoelectron yield spectroscopy measurements of the powder. As a result, we found that $CaZn_2P_2$ would be a promising partner material in photovoltaics based on Zn_3P_2 and $ZnSnP_2$.

Keywords: photovoltaics, solution growth, optoelectronic characterization, buffer layer, emitter

1 Introduction

Towards the multi-terawatt scale implementation of photovoltaic power systems to society, considerable efforts have been devoted to exploring materials for photovoltaic devices (PVs) in the past four decades. While these efforts have led to the development of thin-film PVs with conversion efficiencies over 20%, such as $Cu(In,Ga)Se_2$ (CIGS) [1], CdTe [2], and halide perovskites [3], the use of scarce and/or toxic elements in these devices is considered as a potential risk for large-scale utilization. Various earth-abundant light-absorbing materials have been studied to overcome this issue, but the conversion efficiencies of emerging PVs based on them are still 13% at most [4–7]. One of the bottlenecks for the improvement of earth-abundant thin-film PVs would be the limited choices of partner materials to form a p-n junction with light-absorbing materials (so-called buffer layer or n-type emitter). Emerging PVs are usually constructed by referring to the existing devices; thus, II–VI compounds and TiO_2 are the commonly-used partner materials as we can notice from the recent review article [4]. Probably, for this reason, most of the emerging PVs with relatively high efficiency are based on light-absorbing materials chemically similar to the existing ones (e.g., Cu_2ZnSnS_4 as an alternative to CIGS). In order to practicalize diverse emerging PVs, it is therefore important to explore partner materials.

Zn_3P_2-based PV is an attractive example of emerging PVs because the device with the highest conversion efficiency of 6% was composed of the "Schottky" junction of Zn_3P_2 and Mg, which is different from those of any other PVs [8]. The detailed nature of this device had been controversial for a long period [9–11], but we recently revealed that this is a heterojunction of semiconductors between Zn_3P_2 and $Mg(Mg_xZn_{1-x})_2P_2$, which is formed through the reaction at the Mg/Zn_3P_2 interface [12]. The lattice mismatch between $Mg(Mg_xZn_{1-x})_2P_2$ and Zn_3P_2 is 0.5% at most, and thus, is favorable for photovoltaic applications. On the other hand, Zn_3P_2 has a face-centered cubic (fcc) sublattice of phosphorus, which is often observed in pnictide semiconductors such as InP and $ZnSnP_2$ [13,14]. Therefore, $Mg(Mg_xZn_{1-x})_2P_2$ would be intriguing as a partner material in pnictide-based PVs. Inspired by this discovery, we focused on a related series of compounds, MZn_2P_2 (M: IIA elements such as Ca, Sr, and Ba), in this study.

In order to investigate the properties of MZn_2P_2, we need to deal with the difficulties in their synthesis, i.e.,

* **Corresponding author: Ryoji Katsube,** Department of Materials Science and Engineering, Kyoto University, Kyoto 606-8501, Japan, e-mail: katsube.ryouji.7a@kyoto-u.ac.jp
Yoshitaro Nose: Department of Materials Science and Engineering, Kyoto University, Kyoto 606-8501, Japan

high reactivity and high vapor pressure of each element. As a solution to these problems, we recently proposed the use of Sn as a solvent and successfully investigated the phase equilibria of the Mg-P-Zn system [15]. The solubility of each constituent element in the Sn melt is remarkable [16], which would lead to the reduction of the activities of the elements. Considering also that Sn has a low melting point of 232°C, it can be a suitable solvent for the synthesis of MZn_2P_2. In the present study, we accordingly attempted to prepare MZn_2P_2 bulk crystals using Sn as a solvent and investigate their optoelectronic properties. We then discuss the applicability of MZn_2P_2 as partner materials with pnictide absorbers from the viewpoints of lattice and band parameters.

2 Materials and methods

The starting materials for the growth of MZn_2P_2 crystals were Ba (99% up, chunk), Ca (99%, grain), P (99.9999%, flake), Sn (99.99%, grain), Sr (99%, chunk), and Zn (99.99%, grain). All reagents were purchased from Kojundo Chemical Laboratory Co. Ltd., Japan. Prior to weighing, Sn and Zn were chemically etched in 1/10 diluted hydrochloric acid for 5 min to remove surface oxide layers. They were then sequentially washed with ultrapure water and 2-propanol in an ultrasonic bath for 5 min for each step. Ba and Sr were washed with hexane just before weighing and introducing to the vacuum encapsulation system because they were stored in mineral oil to prevent oxidation. The other materials were used without any preprocessing. The starting materials with the compositions listed in Table 1 were loaded in a carbon (Sankyou Carbon Co., Ltd, Japan) or alumina (99.6%, SSA-S grade, Nikkato Corporation, Japan) crucible and encapsulated in a carbon-coated quartz glass ampule under the pressure of 10^{-2} Pa. Here, a chunk of B_2O_3 was put on the top of the carbon crucible to suppress evaporation of each element by referring to the liquid-encapsulated Czochralski process for the growth of III-V bulk single crystals [17–19]. The samples were denominated as CZP-Sn (M = Ca), SZP-Sn (M = Sr), and BZP-Sn (M = Ba) as shown in Table 1. The ampules were then placed in furnaces, schematically shown in Figure 1(a), for CZP-Sn or 1(c) for SZP-Sn and BZP-Sn, and annealed by the procedures described as follows. The temperature history for CZP-Sn is shown in Figure 1(b). Except for the water quenching steps, the ampules were allowed to stand at a fixed position in the furnace. On the other hand, the furnace for the annealing of SZP-Sn and BZP-Sn was raised with a speed of 5 mm·day^{-1} after homogenization of the samples at 900°C. The temperature profile in the furnace and the initial position of the sample in the furnace are shown in Figure 1(d).

The samples after the heat treatment were cut into plates in the direction perpendicular to the longitudinal direction by a low-speed diamond wheel saw. We here used isoparaffin oil (Lubricant Q purchased from Refine Tec Ltd., Japan) as a lubricant for cutting to suppress decomposition of alkaline-earth compounds via the reaction with water. The sample plates were then mechanically polished by water-resistant abrasive papers while pouring hexane for scanning electron microscopy (SEM) observation and energy-dispersive X-ray spectroscopy (EDS) analysis. Some of the samples were ground into a powder with an agate mortar and pestle for X-ray diffraction (XRD) measurements and optoelectronic analysis.

The compositions of the phases in the ingots were evaluated by SEM-EDS (JCM-6000 Plus equipped with MP-05030-EDK, JEOL Ltd., Japan). The crystal structures of the samples were analyzed by XRD (X'Pert Pro Alpha-1, PANalytical) with a Bragg-Brentano geometry using Cu $K\alpha_1$ incident X-ray from a Johansson-type monochromator. The optical bandgap energies of MZn_2P_2 were evaluated from the Tauc plot of the Kubelka–Munk-transformed diffuse reflectance spectra of powdered specimens [20,21]. The diffuse reflectance spectra were measured by an ultraviolet-visible (UV-Vis) spectrophotometer (UV2600, Shimadzu Corporation, Japan). The ionization potentials (IPs), namely the energy difference between the vacuum level and the valence band maximum of semiconductors, were estimated by photoelectron yield spectroscopy (PYS). The PYS system (BIP-KV201, Bunkoukeiki Co. Ltd., Japan) was calibrated using a Au film as a standard sample right before the measurements.

Table 1: Starting compositions of the samples

Sample No.	Composition (mol%)			
	M	P	Zn	Sn
CZP-Sn (M = Ca)	9	7	24	60
SZP-Sn (M = Sr)	4	8	8	80
BZP-Sn (M = Ba)	4	8	8	80

3 Results and discussion

Figure 2 shows the SEM backscattered electron detector-compositional (BED-C) images and the corresponding EDS mappings of the sample plates containing phosphide phases? Also, the results of EDS quantitative analysis of

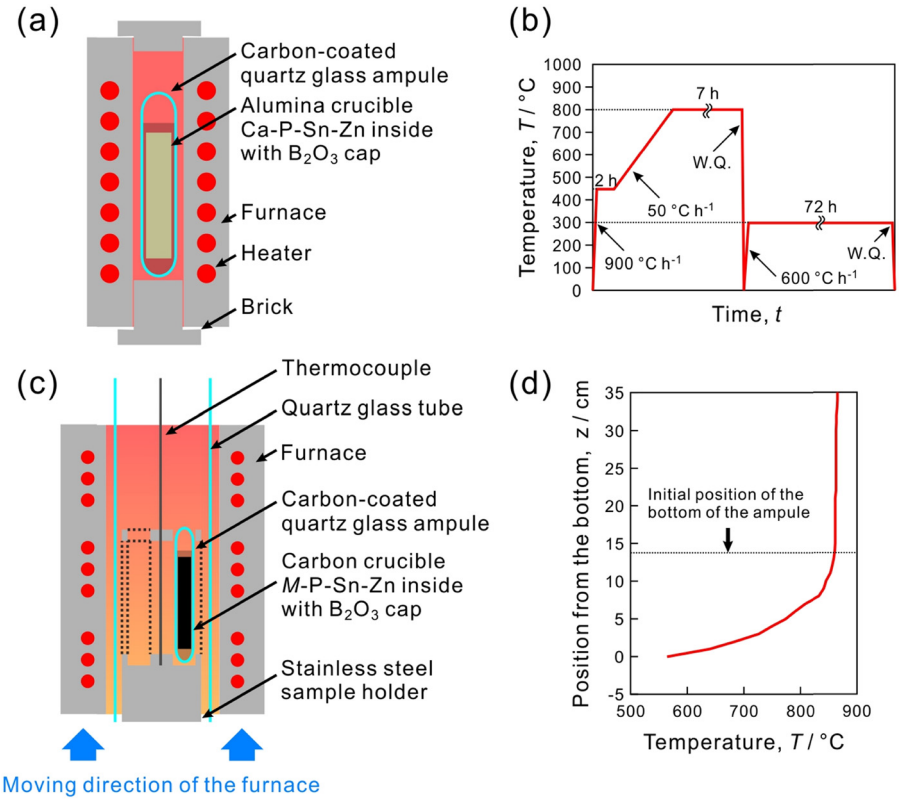

Figure 1: (a) Schematic illustration of the experimental setup and (b) the heat treatment process for the Sn-solution synthesis of $CaZn_2P_2$. (c) Schematic illustration of the Bridgman-type apparatus and (d) temperature profile in the furnace for the Sn-solution synthesis of $SrZn_2P_2$ and $BaZn_2P_2$.

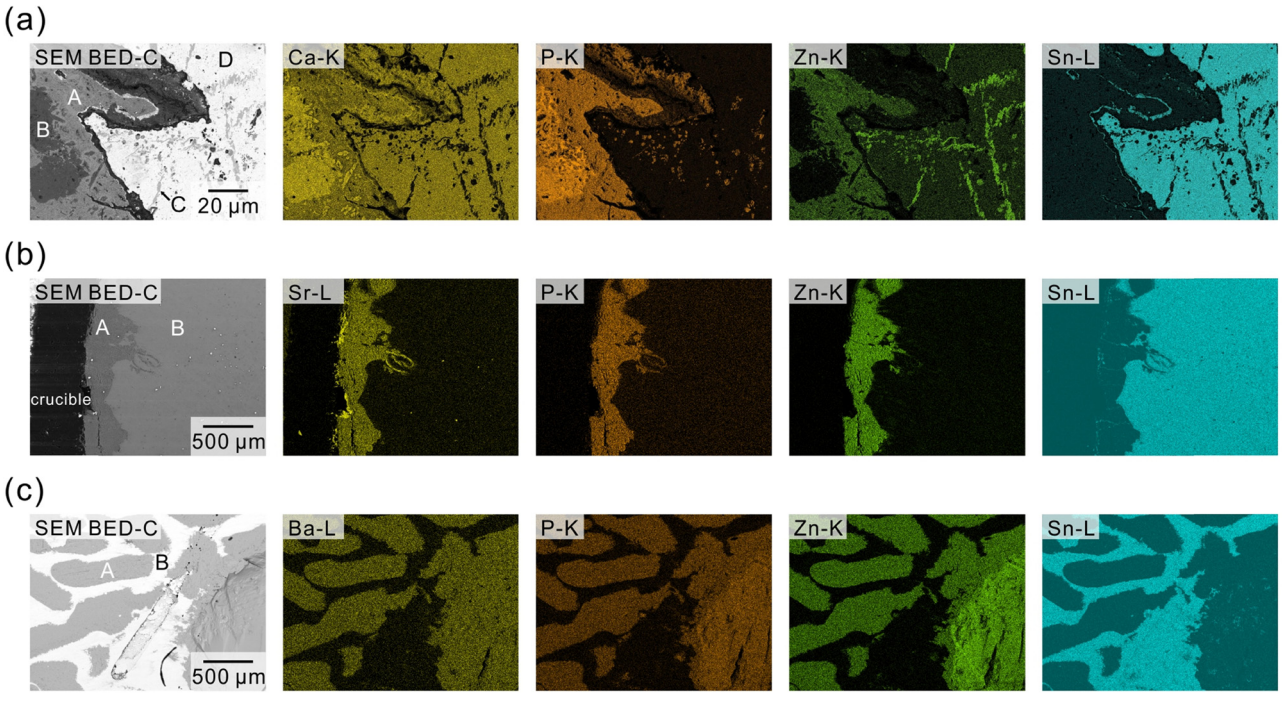

Figure 2: SEM BED-C images and corresponding EDS mappings of the region containing MZn_2P_2 crystals in (a) CZP-Sn, (b) SZP-Sn, and (c) BZP-Sn. The contrast observed in area A at the bottom right of (c) is caused by the inclined shape of the inclined sample surface.

the regions labeled as A–D in the SEM-BED-C images are summarized in Table 2. Two or more regions with different chemical compositions were observed in each sample. The regions denoted as A possess chemical compositions close to the stoichiometry of MZn_2P_2. Here, note that the EDS analysis conducted in this study was semi-quantitative because it was difficult to prepare standard samples for alkaline-earth elements. This would be the reason for the several percent of deviations from the stoichiometry seen in this study, and it remains as future work to investigate off-stoichiometry of MZn_2P_2 phases as in the case for $Mg(Mg_xZn_{1-x})_2P_2$. Another region with the composition with a certain amount of phosphorus was detected in the CZP-Sn (region B), whereas MZn_2P_2 is the only phosphide region in SZP-Sn and BZP-Sn. Zn and Sn are not detected in the EDS profiles of region B in CZP-Sn. The standard deviation in the composition is much larger compared to the other results and the estimated composition is between the stoichiometries of already-known calcium phosphides such as Ca_3P_2 and CaP. We thus assume that this region would be a mixture of them. The other regions should be the solidified flux because they are mainly composed of Sn and Zn.

We then tried to retrieve MZn_2P_2 powder from the sample plates for further analyses because single-phase plates of MZn_2P_2 were unfortunately not obtained as described above. The color of Ca_3P_2 is known to be reddish-brown or gray. This indicates that it might have a bandgap in the near infrared-visible range; therefore, it should be separated as possible from the powder of CZP-Sn to investigate the optoelectronic properties of $CaZn_2P_2$. Fortunately, calcium phosphides are known to be highly reactive with water and oxygen in the atmosphere, and thus, they could be removed from the plates through weathering in the atmosphere for several days. The metallic phases observed in all the samples are relatively ductile and not easily pulverized compared to MZn_2P_2. Utilizing this difference in ductility, we attempted to separate metallic phases and MZn_2P_2 by pounding the sample plates with an agate mortar and pestle. Figure 3 shows the XRD profiles of the powders extracted from CZP-Sn, SZP-Sn, and BZP-Sn through the above-described procedure. The diffraction lines are well indexed with the reference patterns of MZn_2P_2 and Sn. The $CaZn_2P_2$ and the $SrZn_2P_2$ crystals obtained in this study have the trigonal $CaAl_2Si_2$-type structure, which is the same for Mg $(Mg_xZn_{1-x})_2P_2$, and the $BaZn_2P_2$ crystals have the tetragonal

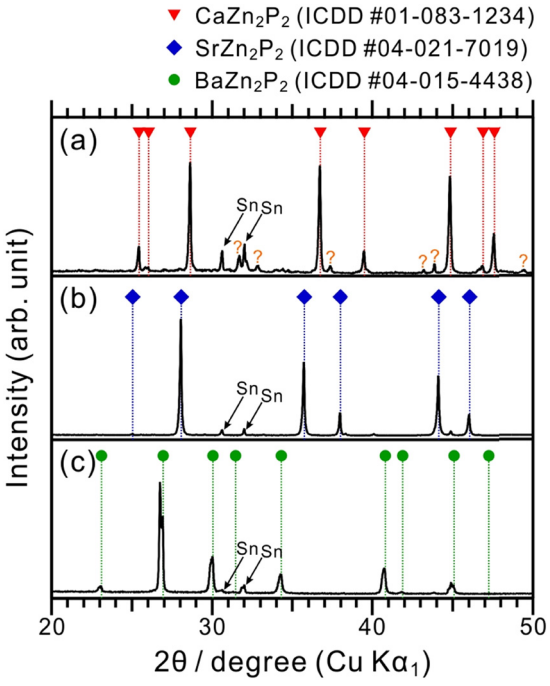

Figure 3: XRD profiles of the powders extracted by pounding and grinding (a) CZP-Sn, (b) SZP-Sn, and (c) BZP-Sn. The diffraction lines denoted by a question mark in (a) could not be identified.

Table 2: Composition of phases observed in Figure 2

Sample no.	Area	Composition (mol%)			
		M	P	Zn	Sn
	A	20.4 ± 2.7	37.5 ± 2.2	41.1 ± 3.2	N.D.
CZP-Sn	B	54.1 ± 12.4	45.9 ± 13.6	N.D.	N.D.
M = Ca	C	N.D.	N.D.	100	N.D.
	D	1.8 ± 0.4	N.D.	17.7 ± 1.3	80.4 ± 1.2
SZP-Sn	A	20.8 ± 0.3	36.2 ± 0.3	43.0 ± 0.2	N.D.
M = Sr	B	N.D.	N.D.	7.9 ± 1.8	92.1 ± 2.2
BZP-Sn	A	18.4 ± 2.0	37.2 ± 0.2	44.1 ± 2.0	0.2 ± 0.1
M = Ba	B	N.D.	N.D.	0.7 ± 0.6	99.3 ± 2.5

N.D.: Not detected.

$ThCr_2Si_2$-type structure. In addition to the signals from these phases, several weak diffraction lines are detected in the XRD profile of the powder from CZP–Sn. These diffractions are probably from decomposition products of calcium phosphides. The intensities of the diffraction lines from MZn_2P_2 are much stronger than those from Sn and the unidentified phase in CZP-Sn; therefore, we could obtain powders mainly composed of MZn_2P_2 from the sample plates.

Subsequently, we evaluated the optoelectronic properties of MZn_2P_2 using the powders extracted for the XRD analysis. Figure 4 summarizes the results of the UV-vis diffuse reflectance analyses of the powders. The data for the powders from CZP–Sn and SZP–Sn are plotted as Tauc plots of the Kubelka–Munk-transformed profiles because they have absorption edges in the measured range of wavelength. According to the profiles, it is revealed that $CaZn_2P_2$ has an indirect fundamental bandgap of 1.85 eV and a direct bandgap of 2.05 eV, and $SrZn_2P_2$ has an indirect fundamental bandgap of 1.70 eV and a direct bandgap of 1.89 eV. In contrast, the diffuse reflectance profile from the BZP-Sn powder does not show any absorption edges. We thus assume that $BaZn_2P_2$ has a metallic or a semimetallic band structure, or a bandgap narrower than 0.9 eV. The above evaluations qualitatively correspond to the calculated band structures in the Materials Project database [22], where $CaZn_2P_2$ and $SrZn_2P_2$ are semiconductors with indirect fundamental bandgaps and slightly wider direct gaps (ID: mp-9569 and mp-8276), and $BaZn_2P_2$ is a semimetal (ID: mp-7426). The characteristics of the optical inter-band transitions in $CaZn_2P_2$ and $SrZn_2P_2$ also agree with the recent computational studies by Murtaza et al. based on the Perdew–Burke–Ernzerhoff generalized gradient approximation (PBE-GGA) with the modified Becke–Johnson (mBJ) potential [23,24], whereas the calculated bandgap of $SrZn_2P_2$ was 0.1 eV larger than that of $CaZn_2P_2$ in contrast to the results in this study. Besides, they reported that the conduction bands of $CaZn_2P_2$ and $SrZn_2P_2$ are mainly composed of the Ca- or the Sr-d orbital and P-p orbital. However, the GGA-mBJ approach is known to give unreliable d-state binding energy [25,26]. This might be the reason for the difference in the bandgap values. In the case of Zintl arsenides ($CaZn_2As_2$ and $SrZn_2As_2$), the density functional theory calculations using a more accurate Heyd–Scuseria–Ernzerhof (HSE06) hybrid functionals were conducted by Xiao et al. [27]. They reported that the bandgap of $CaZn_2As_2$ is larger than that of $SrZn_2P_2$, which coincides with the trend in the phosphides in this study. Also, our result for $BaZn_2P_2$ is consistent with the recent tight-binding linear Muffin-Tin orbital (TB-LMTO) calculation by Balvanz et al. [28]. Here, we should again note that the crystal structure of $BaZn_2P_2$ samples in this study is the well-known $ThCr_2Si_2$-type structure, whereas they reported that there is another polymorph for $BaZn_2P_2$, i.e., the α-$BaCu_2S_2$-type structure. They suggested that the stable polymorph in the temperature range below 850°C should be the α-$BaCu_2S_2$-type one, but we could only obtain $BaZn_2P_2$ crystals with the $ThCr_2Si_2$-type structure with the experimental protocol in this study. We thus suggest further studies are required to draw conclusions on the stability of the polymorphs and phase transformation in $BaZn_2P_2$.

Figure 5 shows the PYS profiles of the powders extracted from CZP-Sn, SZP-Sn, and BZP-Sn. According to Fowler and Kane [29,30], photoelectron yield (Y) is proportional to $(h\nu - \mathrm{IP})^n$ near the threshold, where $h\nu$ is the photon energy and n is the parameter depending on the production and scattering process of photoelectrons. n takes a value in the range from 1 to 3 in the case of semiconductors and it is two for metals. All the PYS spectra in this study show linear dependence on $h\nu$ ($n = 1$) as we can

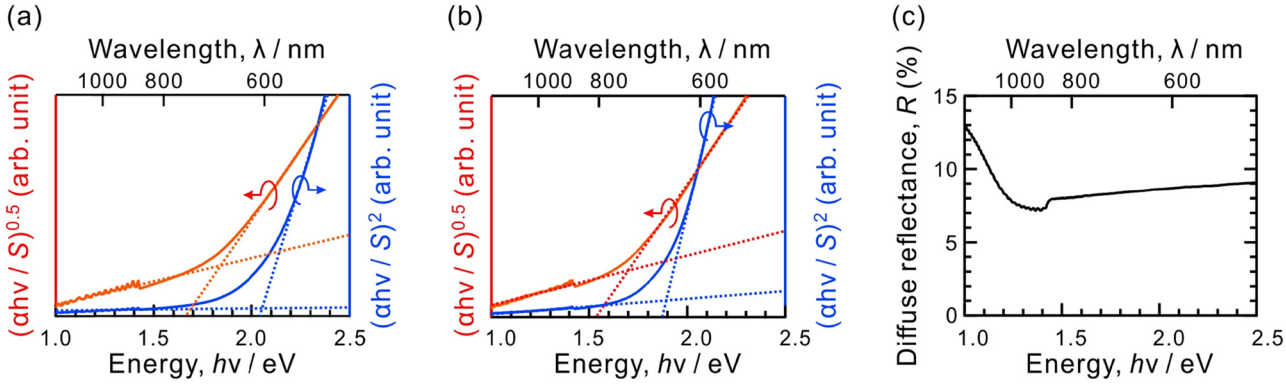

Figure 4: Tauc plots of the Kubelka–Munk-transformed diffuse reflectance of the powders extracted from (a) CZP-Sn ($CaZn_2P_2$) and (b) SZP-Sn ($SrZn_2P_2$). (c) The diffuse reflectance spectrum of the powder extracted from BZP-Sn ($BaZn_2P_2$).

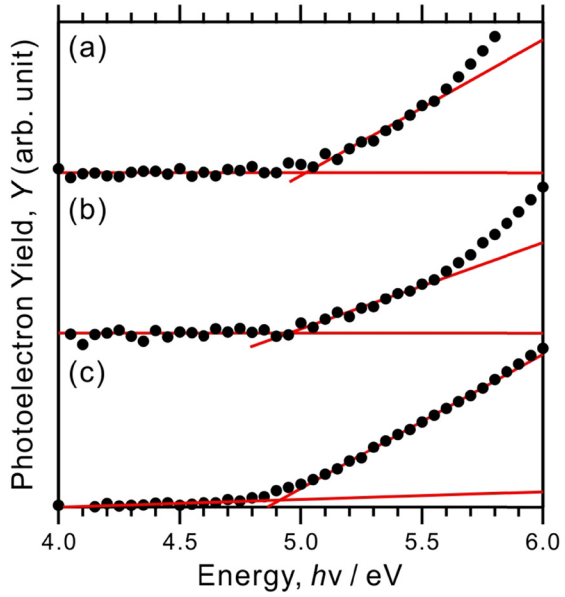

Figure 5: PYS profiles of the powders extracted from (a) $CaZn_2P_2$, (b) $SrZn_2P_2$, and (c) $BaZn_2P_2$.

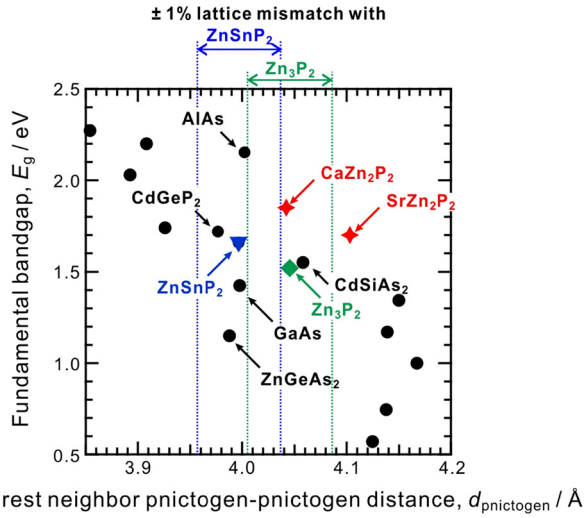

Figure 6: Relationship between the nearest-neighbor pnictogen–pnictogen distance and the fundamental bandgap of various pnictide semiconductors.

see in Figure 5. This indicates that $BaZn_2P_2$ is not a metallic conductor and that the thresholds observed in the spectra correspond to the IPs of MZn_2P_2. Hence, the IPs are evaluated to be 5.0 eV for $CaZn_2P_2$ and $SrZn_2P_2$, and 4.9 eV for $BaZn_2P_2$. Here, we should note that the work function of Sn is 4.42 eV [31], and thus, the PYS spectra are not affected by the secondary phase in powders. These values are close to the IPs of Zn_3P_2 (5.0 eV) calculated from the bandgap (1.5 eV) and the electron affinity (3.5 eV) reported by Nelson et al. [32] and that of $ZnSnP_2$ (5.2 eV) evaluated by our group [33]. Accordingly, the VBM of MZn_2P_2, Zn_3P_2, and $ZnSnP_2$ are aligned within 0.2 eV.

Finally, we discuss the lattice and band matching between MZn_2P_2 and pnictide absorbers such as Zn_3P_2 and $ZnSnP_2$. Figure 6 shows the relationship between nearest-neighbor pnictogen–pnictogen distance, $d_{\text{pnictogen}}$, in pnictogen sublattice in pnictide semiconductors and fundamental bandgap of various pnictide semiconductors. By and large, a downward trend is observed in Figure 6 as is also the case for the bandgap vs lattice constant relationship in semiconductor solid solutions. Considering the bandgap energies and the IPs discussed above, the conduction band minimum of $CaZn_2P_2$ is 0–0.2 eV shallower relative to those of Zn_3P_2 and $ZnSnP_2$. According to the device simulation for the sulfide/CIGS type solar cells by Minemoto et al. [34,35] and Liu and Sites [36], such an offset in the conduction band minimum is in the optimum range for PV applications. On the other hand, pnictogen sublattice in pnictide semiconductors is typically face-centered cubic (fcc, e.g., in InP and GaAs) or hexagonal closed packed (hcp, e.g., GaN) structure; that in MZn_2P_2 is also hcp except for $BaZn_2P_2$. d_{pnictgen} is, therefore, a measure to consider epitaxial lattice mismatch in the orientation relationship where the closest packed planes of the pnictogen sublattice ((111) in fcc and (0001) in hcp) are parallel to each other. Such an orientation relationship was also observed in the $Mg(Mg_xZn_{1-x})_2P_2/Zn_3P_2$ interface in our previous study [12]. As shown in Figure 6, $CaZn_2P_2$ has lattice mismatches of about 1% at most with Zn_3P_2 and $ZnSnP_2$. Therefore, assuming that the discussion for chalcogenide PVs is directly applicable to other types of devices, $CaZn_2P_2$ has a desirable lattice constant and band positions as a partner material in PVs based on Zn_3P_2 and $ZnSnP_2$.

4 Conclusion

We have proven that bulk crystals of MZn_2P_2 (M = Ca, Sr, Ba) can be synthesized from Sn-based solutions, whereas the crystals obtained in this study were embedded in solidified Sn flux. The MZn_2P_2 crystals could be separated from Sn flux sufficiently for optoelectronic characterization by pounding the samples with an agate mortar and pestle. Through the diffuse reflectance and PYS analyses, we revealed that $CaZn_2P_2$ and $SrZn_2P_2$ are semiconductors with indirect bandgaps of 1.85 and 1.70 eV, respectively, and an ionization potential of around 5.0 eV. $BaZn_2P_2$ might be a semiconductor with a narrow bandgap less than 0.9 eV or a semimetal, which corresponds well with the recent calculations. Especially, we found that

$CaZn_2P_2$ would be an appropriate partner material in Zn_3P_2- and $ZnSnP_2$-based PVs from the viewpoints of lattice and band matching. As demonstrated in this study, Sn is an adequate solvent to explore and synthesize compounds including alkaline-earth elements and pnictogens.

Acknowledgments: The authors thank Prof. Fumiyasu Oba, Dr. Kou Harada, and Mr. Tomoya Gake (Tokyo Institute of Technology) for valuable information and fruitful discussions. The authors also thank Prof. Takahiro Wada and Dr. Tsuyoshi Maeda (Ryukoku University) for the measurements by photoelectron yield spectroscopy.

Funding information: This work was financially supported by JST CREST Grant JPMJCR17J2. This work was also supported by the Collaborative Research Project of Laboratory for Materials Structures, Institute of Innovative Research, Tokyo Institute of Technology.

Author contributions: Ryoji Katsube: writing – original draft, review and editing, conceptualization, methodology, investigation; Yoshitaro Nose: writing – review and editing, resource, dupervision, project administration;

Conflict of interest: The authors have no conflicts of interest to declare.

Data availability statement: The data that support the findings of this study are available from the corresponding author on reasonable request. The data are not publicly available due to privacy or ethical restrictions.

References

[1] Nakamura, M., K. Yamaguchi, Y. Kimoto, Y. Yasaki, T. Kato, and H. Sugimoto. Cd-free Cu(In,Ga)$(Se,S)_2$ thin-film solar cell with record efficiency of 23.35%. *IEEE Journal of Photovoltaics*, Vol. 9, No. 6, 2019, pp. 1863–1867.

[2] First Solar Press Release, First Solar builds the highest efficiency thin film PV cell on record, 5 August 2014. https://investor.firstsolar.com/news/press-release-details/2014/First-Solar-Builds-the-Highest-Efficiency-Thin-Film-PV-Cell-on-Record/default.aspx.

[3] Peng, J., D. Walter, Y. Ren, M. Tebyetekerwa, Y. Wu, T. Duong, et al. Nanoscale localized contacts for high fill factors in polymer-passivated Perovskite solar cells. *Science*, Vol. 371, No. 6527, 2021, pp. 390–395.

[4] Zakutayev, A., J. D. Major, X. Hao, A. Walsh, J. Tang, T. K. Todorov, et al. Emerging inorganic solar cell efficiency tables (version 2). *Journal of Physics: Energy*, Vol. 3, No. 3, 2021, id. 032003.

[5] Wang, W., M. T. Winkler, O. Gunawan, T. Gokmen, T. K. Todorov, Y. Zhu, et al. Device characteristics of CZTSSe thin-film solar cells with 12.6% efficiency. *Advanced Energy Materials*, Vol. 4, No. 7, 2018, id. 1301465.

[6] Son, D.-H., S.-H. Kim, S.-Y. Kim, Y.-I. Kim, J.-H. Sim, S.-N. Park, et al. Effect of solid-H_2S gas reactions on CZTSSe thin film growth and Photovoltaic properties of a 12.62% efficiency device. *Journal of Materials Chemistry A*, Vol. 7, No. 44, 2019, pp. 25279–25289.

[7] Sanehira, E. M., A. R. Marshall, J. A. Christians, S. P. Harvey, P. N. Ciesielski, L. M. Wheeler, et al. Enhanced mobility $CsPbI_3$ quantum dot arrays for record-efficiency, high-voltage photovoltaic cells. *Science Advances*, Vol. 3, No. 10, 2017, id. eaao4204.

[8] Bhushan, M. and A. Catalano. Polycrystalline Zn_3P_2 schottky barrier solar cells. *Applied Physics Letters*, Vol. 38, No. 1, 1981, pp. 39–41.

[9] Catalano, A. and M. Bhushan. Evidence of p/n homojunction formation in Zn_3P_2. *Applied Physics Letters*, Vol. 37, No. 6, 1980, pp. 567–69.

[10] Kimball, G. M., N. S. Lewis, and H. A. Atwater. Mg doping and alloying in Zn_3P_2 heterojunction solar cells. In *Proceedings of the 35th IEEE Photovoltaic Specialists Conference (PVSC), June 20–25, 2010*, IEEE, 2010, pp. 1039–1043.

[11] Kimball, G. M., N. S. Lewis, and H. A. Atwater. Direct evidence of Mg–Zn–P alloy formation in Mg/Zn_3P_2 solar cells. In *Proceedings of the 037th IEEE Photovoltaic Specialists Conference (PVSC), June 19–24, 2011*, IEEE, 2011, id. 003381.

[12] Katsube, R., K. Kazumi, T. Tadokoro, and Y. Nose. Reactive epitaxial formation of a Mg–P–Zn ternary semiconductor in Mg/Zn_3P_2 solar cells. *ACS Applied Materials and Interfaces*, Vol. 10, No. 42, 2018, pp. 36102–36107.

[13] Giesecke, G. and H. Pfister. Präzisionsbestimmung der Gitterkonstanten von $A^{III}B^{V}$-Verbindungen. *Acta Crystallographica*, Vol. 11, No. 5, 1958, pp. 369–371.

[14] Shay, J. L. and J. H. Wernick. Chapter 2 – The chalcopyrite structure and crystal growth. In *Ternary Chalcopyrite Semiconductors: Growth, Electronic Properties, and Applications*, Pergamon Press, Oxford, United Kingdom, 1975, pp. 3–78.

[15] Katsube, R. and Y. Nose. Experimental investigation of phase equilibria around a ternary compound semiconductor $Mg(Mg_xZn_{1-x})_2P_2$ in the Mg–P–Zn system at 300°C using Sn flux. *Journal of Solid State Chemistry*, Vol. 280, 2019, id. 120983.

[16] Massalski, T. B. and ASM International. *Binary alloy phase diagrams*. ASM International, 1990.

[17] Metz, E. P. A., R. C. Miller, and R. A. Mazelsky. Technique for pulling single crystals of volatile materials. *Journal of Applied Physics*, Vol. 33, No. 6, 1962, pp. 2016–2017.

[18] Mullin, J. B., B. W. Straughan, and W. S. Brickell. Liquid encapsulation techniques: the use of an inert liquid in suppressing dissociation during the melt-growth of InAs and GaAs crystals. *Journal of Physics and Chemistry of Solids*, Vol. 26, No. 4, 1965, pp. 782–84.

[19] Bass, S. J. and P. E. Oliver. Pulling of gallium phosphide crystals by liquid encapsulation. *Journal of Crystal Growth*, Vol. 3–4, 1968, pp. 286–90.

[20] Kubelka, P. and F. Munk. Ein beitrag zur optik der farbanstriche. *Zeitschrift Für Technische Physik*, Vol. 12, 1931, pp. 593–601.

[21] Tauc, J. Optical properties and electronic structure of amorphous Ge and Si. *Materials Research Bulletin*, Vol. 3, No. 1, 1968, pp. 37–46.
[22] Jain, A., S. P. Ong, G. Hautier, W. Chen, W. D. Richards, S. Dacek, et al. Commentary: the materials project: a materials genome approach to accelerating materials innovation. *APL Materials*, Vol. 1, No. 1, 2013, id. 011002.
[23] Murtaza, G., N. Yousaf, M. Yaseen, A. Laref, and S. Azam. Systematic studies of the structural and optoelectronic characteristics of $CaZn_2X_2$(X = N, P, As, Sb, Bi). *Materials Research Express*, Vol. 5, No. 1, 2018, id. 016304.
[24] Murtaza, G., N. Yousaf, A. Laref, and M. Yaseen. Effect of varying pnictogen elements (Pn = N, P, As, Sb, Bi) on the optoelectronic properties of $SrZn_2Pn_2$. *Zeitschrift Für Naturforschung A*, Vol. 73, No. 4, 2018, pp. 285–293.
[25] Singh, D. J. Electronic structure calculations with the Tran-Blaha modified Becke-Johnson density functional. *Physical Review B*, Vol. 82, No. 20, 2010, id. 205102.
[26] Jiang, H. Band gaps from the Tran-Blaha modified Becke-Johnson approach: a systematic investigation. *The Journal of Chemical Physics*, Vol. 138, No. 13, 2013, id. 134115.
[27] Xiao, Z., H. Hiramatsu, S. Ueda, Y. Toda, F. Y. Ran, J. Guo, et al. Narrow bandgap in β-$BaZn_2As_2$ and its chemical origins. *Journal of the American Chemical Society*, Vol. 136, No. 42, 2014, pp. 14959–14965.
[28] Balvanz, A., S. Baranets, M. O. Ogunbunmi, and S. Bobev. Two polymorphs of $BaZn_2P_2$: crystal structures, phase transition, and transport properties. *Inorganic Chemistry*, Vol. 60, No. 18, 2021, pp. 14426–35.
[29] Fowler, R. H. The analysis of photoelectric sensitivity curves for clean metals at various temperatures. *Physical Review*, Vol. 38, No. 1, 1931, pp. 45–56.
[30] Kane, E. O. Theory of photoelectric emission from semiconductors. *Physical Review*, Vol. 127, No. 1, 1962, pp. 131–41.
[31] Simmons, J. G. Intrinsic fields in thin insulating films between dissimilar electrodes. *Physical Review Letters*, Vol. 10, No. 1, 1963, pp. 10–12.
[32] Nelson, A. J., L. L. Kazmerski, M. Engelhardt, and H. Hochst. Valence-band electronic structure of Zn_3P_2 as a function of annealing as studied by synchrotron radiation photoemission. *Journal of Applied Physics*, Vol. 67, No. 3, 1990, pp. 1393–1396.
[33] Kuwano, T., R. Katsube, K. Kazumi, and Y. Nose. Performance enhancement of $ZnSnP_2$ solar cells by a Cu_3P back buffer layer. *Solar Energy Materials and Solar Cells*, Vol. 221, 2021, id. 110891.
[34] Minemoto, T., Y. Hashimoto, T. Satoh, T. Negami, H. Takakura, and Y. Hamakawa. $Cu(In,Ga)Se_2$ solar cells with controlled conduction band offset of window/$Cu(In,Ga)Se_2$ layers. *Journal of Applied Physics*, Vol. 89, No. 12, 2001, pp. 8327–8330.
[35] Minemoto, T., T. Matsui, H. Takakura, Y. Hamakawa, T. Negami, Y. Hashimoto, et al. Theoretical analysis of the effect of conduction band offset of window/CIS layers on performance of CIS solar cells using device simulation. *Solar Energy Materials and Solar Cells*, Vol. 67, No. 1, 2001, pp. 83–88.
[36] Liu, X. and J. R. Sites. Calculated effect of conduction-band offset on $CuInSe_2$ solar-cell performance. *AIP Conference Proceedings*, Vol. 353, 1996, pp. 444–452.